OPTICS CORRECTION FOR FOURTH-GENERATION LIGHT SOURCES AND FUTURE COLLIDERS

E. Musa*, I. Agapov, K. Paraschou, J. Keil,
Deutsches Elektronen-Synchrotron DESY, Hamburg, Germany
S. M. Liuzzo, S. White, European Synchrotron Radiation Facility, Grenoble, France
S. Habet, Synchrotron SOLEIL, Gif-sur-Yvette, France

Abstract

Accurate lattice-optics correction is essential for achieving the design performance of modern light sources and future circular colliders targeting ultra-low emittances. Such machines rely on strong magnets that are highly sensitive to field and alignment errors. In this work, we investigate approaches for the correction of the linear optics of several accelerators. The study includes selecting appropriate correction steps, defining the fitted parameters, and designing optics correction schemes tailored to the characteristics of each accelerator. Experimental tests were performed at ESRF-EBS, while the simulation studies for PETRA IV, FCC-ee and SOLEIL II investigate the achievable performance of future machines.

CHALLENGES IN LOW-EMITTANCE STORAGE RINGS

The pursuit of developing modern fourth-generation light sources and future circular colliders presents significant challenges. In synchrotron light sources, the performance is characterized by the brilliance [1] of the emitted radiation, which scales inversely with the transverse beam emittances. Similarly, future circular colliders aim to maximize luminosity [2], requiring extremely small beam sizes at the interaction points. Strong focusing and sextupoles required for ultra-low emittance increase the sensitivity to alignment and field errors. In particular, strong sextupoles introduce feed-down effects that further complicate the control of the linear optics under tight alignment tolerances, ultimately impacting the overall machine performance.

Figure 1 illustrates the sensitivity of the FCC-ee at Z energy lattice to unrealistically small transverse alignment errors in both the arc and Interaction Region (IR). For an alignment error of 1 µm, the vertical RMS beta-beating increases significantly to approximately 30% in the IR, demonstrating the high sensitivity of the optics to small misalignments.

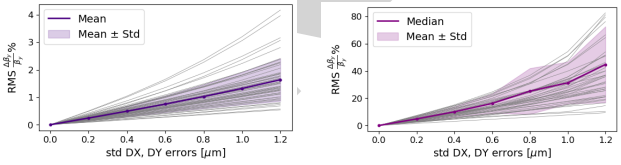

Figure 1: Optics sensitivity to transverse alignment errors for the FCC-ee Z-energy lattice [3].

* elaf.musa@desy.de

OPTICS CORRECTION METHODS

A number of optics correction algorithms and techniques have been developed, including K-modulation, Turn-by-Turn (TbT) beam excitation measurements, and Orbit Response Matrix (ORM)-based methods such as LOCO [4]. Although successfully applied in several accelerators, the K-modulation [5] method can become time consuming for HMBA lattices due to the large number of quadrupoles requiring individual variation.

Optics correction techniques based on TbT beam centroid measurements are widely used, particularly in circular colliders [6]. However the experimental test of these approach in light sources might be limited by hardware problems [7].

LOCO has become a standard tool for optics correction, particularly in synchrotron light sources [8–10]. For machines with strong focusing and complex lattice structures, such as Hybrid Multi-Bend Achromats (HMBA), the correction problem becomes increasingly challenging due to parameter degeneracy and strong correlations between lattice elements.

A comprehensive review of optics correction techniques and their evolution is presented in Ref. [11].

LOCO solves a non-linear least-squares problem by iteratively updating lattice parameters using ORM measurement together with Singular Value Decomposition (SVD) technique as described in Ref. [4]. Strong quadrupole correlations can lead to non-physical solutions.

To mitigate this degeneracy, additional constraints are introduced to regularize the solution. The modified χ^2 function is given by (see Ref. [12] for details):

$$\chi^2 = \sum_{i,j} \frac{\left(C_{\mathrm{mod},ij} - C_{\mathrm{meas},ij}\right)^2}{\sigma_i^2} + \frac{1}{\sigma_{\Delta K}^2} \sum_k w_k^2 \left(\Delta K_k\right)^2, \quad (1)$$

where the second term penalizes large variations of selected quadrupole strengths. The weights w_k allow targeted regularization. Within the Levenberg–Marquardt [13] framework, the parameter update formula becomes:

$$\left(J^T W J + \lambda I + G^T G\right) \Delta \mathbf{p} = J^T W \left(C_{\mathrm{meas}} - C_{\mathrm{mod}}\right), \quad (2)$$

where J is the Jacobian matrix, and W includes the BPMs noise, and G is the constraint matrix defined as

$$G = \mathrm{diag}\left(\frac{w_k}{\sigma_{\Delta K}}\right). \quad (3)$$

Table 1: Error Model for PETRA IV

Component	Errors
Magnets	Transverse offsets: 30 µm Rolls: 200 µrad Calibration : 0.05% (Quads), 0.1% (rest)
Girders	Transverse offsets (endpoints): 150 µm Rolls: 200 µrad
BPMs	Transverse offsets: 500 µm Rolls: 400 µrad Noise: 0.1 µm (orbit), 50 µm (TbT) Calibration: 5%
Correctors	Rolls: 200 µrad Calibration: 2%

This formulation enables a controlled reduction of parameter degeneracy and leads to more stable and physically meaningful optics correction.

ERROR ASSUMPTIONS

The studies are performed using a unified Python-based simulation framework based on `pySC` [14], a simulated commissioning toolkit used to introduce errors, generate measurement data, and apply a wide range of correction techniques, together with `pyLOCO` [15], a Python framework for lattice parameters fitting. This softwares development is aligned with ongoing efforts toward a Python Accelerator Middle Layer (pyAML) [16].

Error Model

Table 1 summarizes the error model used in the `pySC` framework for PETRA-IV simulations.

Correction Configuration

The linear optics correction follows a standard commissioning sequence, which can be adapted depending on the machine conditions:

- First- or second-turn threading
- Trajectory beam-based alignment (BBA)
- Multipoles ramp-up with intermediate trajectory correction
- Orbit beam-based alignment (BBA)
- Chromaticity and orbit/tune correction
- Linear optics correction

Figure 2 shows the DA for 100 seeds after standard commissioning procedures and prior to linear optics correction. A large reduction of the DA is observed, demonstrating that commissioning alone is insufficient to restore the machine performance and that dedicated linear optics correction is essential.

ACHIEVABLE PERFORMANCE

PETRA IV

PETRA IV will upgrade PETRA III into an ultra-low-emittance storage ring, with 2.3 km circumference, reducing

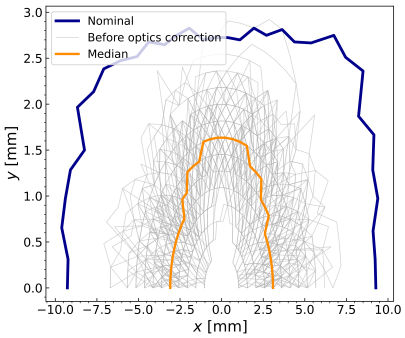

Figure 2: DA for 100 PETRA IV seeds after commissioning and before linear optics correction.

the horizontal emittance by a factor of 65 (20 pm) and providing up to 500 times higher X-ray brightness [17, 18]. The PETRA IV lattice consists of approximately 1350 normal quadrupoles, 432 sextupoles, 786 BPMs, and 1438 horizontal and vertical orbit correctors.

Using the error model summarized in Table 1. A set of 100 seeds is generated and processed through the commissioning simulation sequence described previously. The following results illustrate the performance of the linear optics correction after the application of these standard commissioning steps.

LOCO Setup All normal quadrupoles and 388 fast orbit correctors are used for beta beating and coupling correction respectively, which was found to provide the best performance among the tested quadrupoles configurations. The ORM is constructed using all BPMs. For computational efficiency, a subset of 10 horizontal and 10 vertical orbit correctors is selected.

Dispersion is included in the fit with a properly selected weight. The LOCO fit was performed in multiple stages. In each stage, a number of iterations were applied, with a new ORM measurement performed after each applied correction. The corresponding fitted parameters are summarized in Table 2. Optimal SVD cut-offs were found near 2500 and 1750. The LOCO fit is performed using the Levenberg–Marquardt algorithm with a damping parameter $\lambda = 10^{-3}$.

Due to the strong correlations between PETRA IV quadrupoles, a constrained fitting approach was found to be necessary. This was implemented by introducing weights on the quadrupole strengths, guided by a Jacobian analysis used to determine the corresponding weights. The application of the constrained fit significantly reduces the RMS variation of the quadrupoles and skew correctors while maintaining good optics performance, as shown in Fig. 3. The resulting correction strengths remain moderate and consistent with operational constraints.

Figure 4 shows the global optics improvement, including the achieved DA and local momentum acceptance.

ESRF-EBS

The ESRF-EBS studies constitute the experimental part of this work. Linear optics correction tests were performed

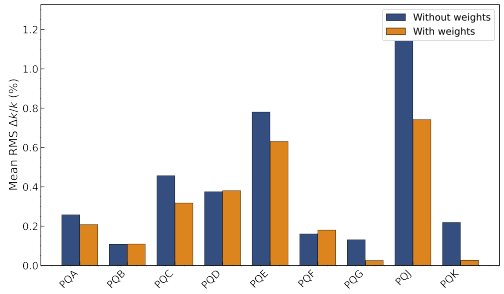

Figure 3: Comparison of the mean RMS normal quadrupole strength variation per family with and without constrained LOCO fit for PETRA IV.

Table 2: LOCO Fitting Strategy for PETRA IV

Stage	Fitted parameters	Matrix terms
1	Quads, BPM gains, COR cal.	Diagonal
2	Skew quads, BPM/COR coupling	Off-diagonal

Table 3: Comparison of LOCO correction strategies applied to the ESRF-EBS, and the resulting measured emittances after applying one iteration of correction. "Gains" refer to horizontal and vertical BPM and corrector calibrations, while "Coup." denotes BPM coupling terms. In case (C), BPM coupling is included together with the skew quadrupole fit. The label "thr" indicates a threshold-based SVD selection, where singular values are retained relative to the maximum singular value using a threshold of 10^{-2}.

Case	Gains	Coup.	QDs	Skew	ϵ_x [pm rad]	ϵ_y [pm rad]
Before	–	–	–	–	157 ± 8	7.35 ± 0.60
A	100	0	64	32	144 ± 8	0.33 ± 0.30
B	thr	thr	64	32	144 ± 8	1.93 ± 0.40
C	100	0	85	50	144 ± 8	0.12 ± 0.30
D	thr	thr	96	10	148 ± 8	2.23 ± 0.40

experimentally at ESRF-EBS [19] after a machine restart following realignment [20]. The measurement conditions are described in Ref. [15]. Different LOCO fit strategies were applied, varying both the SVD spectrum cut-off selection and the order of fitted parameters. Dispersion was included together with the orbit response matrices, with a weight of 5, and 3 BPMs were excluded from the analysis. The optics correction focuses on quadrupoles located in the immediate vicinity of sextupoles, providing a local compensation of sextupoles errors. For coupling errors, the correction is applied globally using all available skew quadrupoles. Table 3 summarizes the configurations together with the resulting measured horizontal and vertical emittances after one applied correction.

All tested LOCO fit strategies reduced the vertical emittance. However, the final performance strongly depends on the SVD selection. The threshold-based approaches (cases B and D) result in a more conservative correction due to strong parameter degeneracy, which leads to the inclusion of small singular value modes in the fit. Among the tested configurations, case C provides the best performance, achieving a vertical emittance of 0.12 ± 0.30 pm rad after one correction iteration. A second correction was performed using this configuration.

Nevertheless, case A already achieves a comparable optics correction with significantly lower correction strength, as shown in Fig. 5, making it efficient candidate for routine operation. Figures 6 show the reduction of dispersion and beta beating after applying two correction iterations following (case C), the achieved horizontal and vertical emittance after two iterations were 149 ± 8 pm rad and 0.99 ± 030 pm rad respectively.

SOLEIL II

The SOLEIL upgrade has a circumference of 353.92 m. It aims to reduce the horizontal emittance from 4 nm rad to 85 pm rad at 2.75 GeV [21]. A total of 372 normal corrector coils and 134 skew quadrupoles are used for the linear optics correction. The error model presented in [22] is used. Sextupoles are kept on, and commissioning simulation is performed within `pySC`, including first-turn trajectory correction, BBA, orbit and tune correction, and finally LOCO using the `pyLOCO` software.

A threshold-based SVD cut-off was efficient for optics correction. The initial optics conditions prior to linear optics correction and the results after correction are summarized in Table 4.

We investigated two approaches for applying LOCO. The SOLEIL II lattice includes 372 normal corrector coils and 162 normal quadrupoles. The impact of the quadrupole selection in the LOCO fit is examined.

A lattice including calibration errors of 0.2% on the normal quadrupoles and BPM noise of 10 µm is used. In option 1, a baseline set of normal correctors is fitted using LOCO, and the resulting corrections are directly applied to the error lattice. In option 2, the number of fitted elements is increased to include both the correctors and the normal quadrupoles. The fitted lattice obtained from Option 2 is used as the starting point for a second fit, based on response matrices constructed from phase advances between nearby BPMs. In this stage, only quadrupole correctors are included in the fit. The resulting corrections are then applied to the initial error lattice. The impact of the two fit strategies in the achieved beta-beating is illustrated in Fig. 7.

Table 4: Summary of optics correction results after LOCO at SOLEIL II.

Observable	Before	After
RMS orbit H / V [µm]	31.83 / 31.45	30.33 / 33.79
RMS $\Delta\beta_{x/y}/\beta_{x/y}$ [%]	8.58 / 13.56	2.02 / 1.92
Median ε_x [pm] / ε_y [pm]	83.15 / 8.89	85.87 / 1.30

FCC-ee

The minimization of phase advance and coupling RDTs using the corresponding response matrices, as described in Ref. [11], is used for the linear optics correction of the FCC-ee W-energy lattice for both the GHC and LCC [23,24] optics designs. The correction is applied following the detailed

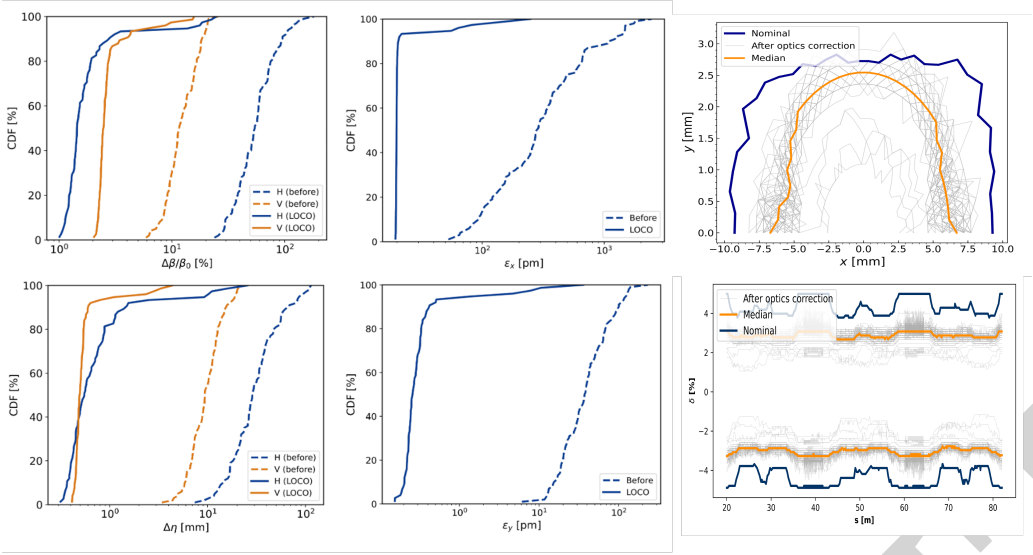

Figure 4: Performance of LOCO correction for PETRA IV over 100 commissioning simulation seeds, achieving median horizontal and vertical emittances of 19.87 pm and 0.26 pm, respectively.

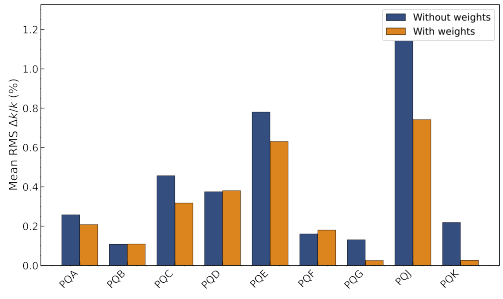

Figure 5: Fitted integrated strength variations ΔKL for normal (left) and skew (right) quadrupoles after LOCO for Cases A–D for EBS.

commissioning simulation sequence described earlier within the pySC framework. The simulations are performed using the error assumptions summarized in Table 5. A measurement noise of 10 µm is assumed for the dispersion measurements, while the phase advance measurements are assumed to have a precision of 1×10^{-4}. The resulting optics performance after correction is summarized in Table 6. The recovery of the DA for multiple seeds are shown in Fig. 8.

Table 5: Error Assumptions in the FCC-ee (W) Simulations

Element	$\sigma_{x/y}$ **[µm]**	σ_θ **[µrad]**	$\Delta K/K$
Arc quads & sext.	50	50	2×10^{-4}
Dipoles	1000	1000	10×10^{-4}
Girders	150	150	—
BPMs	10	—	—

We investigated the application of LOCO for FCC-ee using pyLOCO using a reduced error model. To reduce the computational cost associated with the large collider circumference (~ 91 km) and the large number of lattice components, a reduced set of 10 horizontal and 10 vertical correctors distributed around the ring was used. The LOCO correction was performed iteratively using a Levenberg–Marquardt algorithm while fitting BPM, corrector, and quadrupole calibration errors. The correction significantly reduced beta

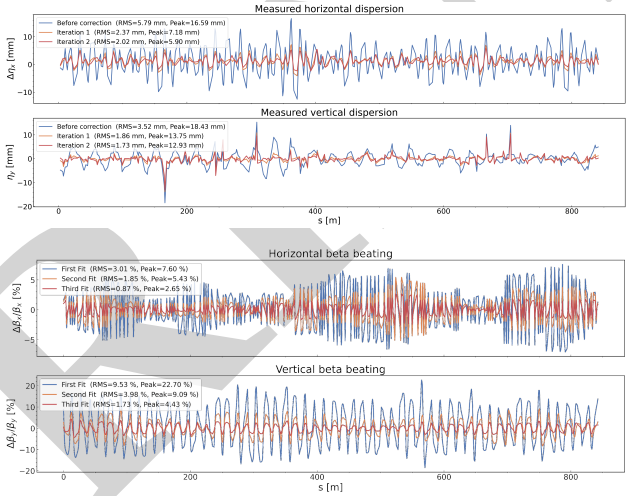

Figure 6: Top: horizontal and vertical dispersion. Bottom: horizontal and vertical beta beating after two LOCO correction iterations using pyLOCO at ESRF-EBS. The spikes observed in the dispersion are associated with BPM calibration and coupling errors. These spikes were observed on the LOCO fit result when coupling was mainly fitted through the BPM coupling.

beating and dispersion, as shown in Fig. 9, together with good reconstruction of the fitted calibration errors, indicating the feasibility of applying LOCO to large-scale future collider lattices such as FCC-ee.

DISCUSSION

The studies presented in this work demonstrate the increasing need for robust linear optics correction schemes for modern fourth-generation light sources and future circular colliders. Optics correction studies were performed for a broad range of accelerators, from compact low-emittance storage rings such as SOLEIL II, to intermediate-scale HMBA lattices including PETRA IV and ESRF-EBS, and up to very

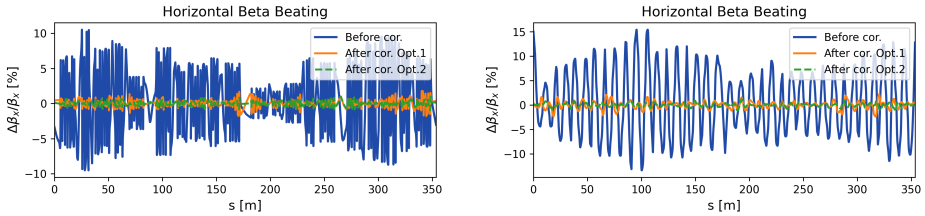

Figure 7: Beta beating before and after correction for the two LOCO fit options for SOLEIL II. The optics correction reduces the beta beating in both planes. The initial RMS beta beating of 4.32% (horizontal) and 6.59% (vertical) is reduced to 0.55% and 0.76% using option 1, and further improved to 0.33% and 0.39% with option 2.

Table 6: FCC-ee (W) Commissioning Simul. Results [25]

Observable	**GHC**	**LCC**
Orbit RMS [µm]	89.3 / 98.4	101.9 / 87.7
Quad. corr. [mT]	1.18 / 1.33	0.16 / 0.13
$\Delta D_{x/y}$ [mm]	5.19 / 0.64	0.12 / 0.52
Phase adv. [$10^{-4}2\pi$]	4.0 / 12.0	0.73 / 0.65
$\Delta\beta_{x/y}/\beta_{x/y}$ [%]	0.4 / 1.2	0.11 / 0.11
$\lvert f_{1001}\rvert/\lvert f_{1010}\rvert$ [10^{-4}]	0.12 / 0.02	1.02 / 0.06
ε_x [nm] / ε_y [pm]	2.24 / 3.58	2.07 / 0.46

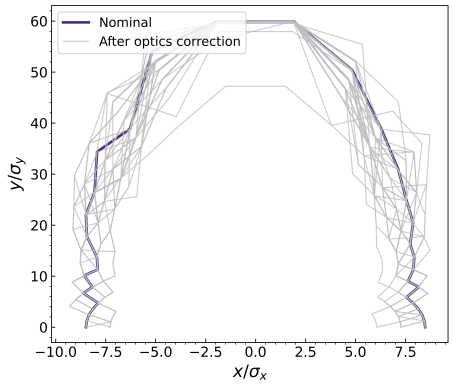

Figure 8: Recovery of the DA for the FCC-ee LCC optics after optics correction.

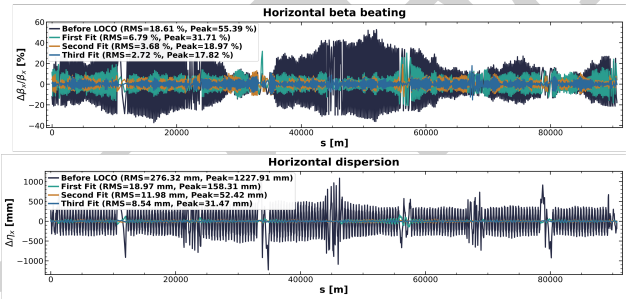

Figure 9: Example of LOCO correction performance for the FCC-ee (LCC) lattice. Top: horizontal beta beating before correction and after successive LOCO iterations. Bottom: horizontal dispersion deviation before correction and after successive LOCO iterations.

large-scale collider lattices such as FCC-ee. The results demonstrate that LOCO remains a powerful approach across very different accelerator scales and lattice configurations.

The computational cost was reduced through reduced ORM configurations and parallelized Jacobian calculations. For large-scale applications, the repeated recalculation of the Jacobian using the updated disturbed model during the LOCO fit iterations, particularly for quadrupole parameters, represents the dominant computational cost. This limitation could be mitigated by calculating the ORM using linear transfer matrix formulas and computing the Jacobian once from the initial model and reusing it during the fitting process, although this may slightly affect the final correction accuracy. Further optimization, including improved parameter selection approaches, will be investigated in future studies.

The studies also highlight the importance of carefully tuning the fit configuration, including the choice of fitted parameters at each iteration, the SVD cut-off strategy, and the use of constrained fitting techniques. In particular, constrained fitting plays an essential role in controlling parameter degeneracy and maintaining realistic correction strengths. The experimental studies at ESRF-EBS further demonstrate the applicability of the developed framework to real machine operation, in addition to simulation.

ACKNOWLEDGMENT

The authors would like to thank X. Huang for the fruitful discussions on constrained fitting techniques. We also thank R. Tomás and J. Keintzel for the insightful discussions and valuable information exchange on the FCC-ee optics tuning.

REFERENCES

[1] R. P. Walker, "Undulator radiation brightness and coherence near the diffraction limit," *Phys. Rev. Accel. Beams*, vol. 22, p. 050704, 2019. doi:10.1103/PhysRevAccelBeams.22.050704

[2] W. Herr and B. Muratori, "Concept of luminosity," CERN Accelerator School, Geneva, Switzerland, Rep. CERN-2006-002, pp. 361–388, 2006. doi:10.5170/CERN-2006-002.361

[3] E. Musa, "Optics measurement and correction for future electron circular colliders," Ph.D. dissertation, University of Hamburg, Hamburg, Germany, 2024. https://ediss.sub.uni-hamburg.de/handle/ediss/11391

[4] J. Safranek and M. Lee, "Calibration of the X-ray ring quadrupoles, BPMs, and orbit correctors using the measured orbit response matrix," CERN, Geneva, Switzerland,

Rep. SLAC-PUB-6442. https://cds.cern.ch/record/262081

[5] A. Hofmann and B. Zotter, "Measurement of the beta-functions in the ISR," CERN ISR-TH-AH-BZ/amb Report, Runs 640–642, 1975. https://cds.cern.ch/record/1131122/files/CM-P00072144.pdf

[6] J. Borer, A. Hofmann, J.-P. Koutchouk *et al.*, "Measurements of betatron phase advance and beta function in the ISR," *IEEE Trans. Nucl. Sci.*, vol. 30, p. 2406, 1983. doi:10.1109/TNS.1983.4332913

[7] I. Agapov *et al.*, "Linear and nonlinear optics analysis from multi-turn data at PETRA III," in *Proc. IPAC'17*, Copenhagen, Denmark, May 2017, paper MOPAB040. doi:10.18429/JACoW-IPAC2017-MOPAB040

[8] R. F. Ximenes Resende, L. Liu, M. Plotegher, and P. Tavares, "Analysis of the LNLS storage ring optics using LOCO," in *Proc. PAC'09*, Vancouver, Canada, May 2009, paper TH6PFP012, pp. 3720–3722.

[9] I. Martin, M. Abbott, R. Bartolini, M. Furseman, and G. Rehm, "A fast optics correction for the Diamond storage ring," in *Proc. IPAC'14*, Dresden, Germany, Jun. 2014. doi:10.18429/JACoW-IPAC2014-TUPRI083

[10] G. Benedetti, D. Einfeld, Z. Martí, and M. Muñoz, "LOCO in the ALBA storage ring," in *Proc. IPAC'11*, San Sebastián, Spain, Sep. 2011, pp. 2055–2057. doi:10.13140/2.1.2956.4164

[11] R. Tomás *et al.*, "Review of linear optics measurement and correction for charged particle accelerators," *Phys. Rev. Accel. Beams*, vol. 20, p. 054801, 2017. doi::10.1103/PhysRevAccelBeams.20.054801

[12] X. Huang, J. Safranek, and G. Portmann, "LOCO with constraints and improved fitting technique," in *Proc. PAC'05*, Knoxville, TN, USA, May 2005, pp. 3652–3654.

[13] J. J. Moré, "The Levenberg–Marquardt algorithm: implementation and theory," *Lect. Notes Math.*, vol. 630, pp. 105–116, 1978. doi:10.1007/BFb0067700

[14] K. Paraschou *et al.*, "Tests of commissioning simulation tools in operation of storage ring light sources," presented at IPAC'26, Deauville, France, May 2026, paper WEP5076, this conference.

[15] E. Musa *et al.*, "pyLOCO: A Python framework for linear optics correction in storage rings," presented at IPAC'26, Deauville, France, May 2026, paper WEP5011, this conference.

[16] Python Accelerator Middle Layer developers, "Python Accelerator Middle Layer," 2026. https://pyaml.readthedocs.io/en/latest/

[17] C. Schroer, R. Wanzenberg, I. Agapov, *et al.*, "PETRA IV: the ultralow-emittance source project at DESY," *J. Synchrotron Rad.*, vol. 26, no. 5, pp. 1277–1290, 2019. doi:10.1107/S1600577518008858

[18] I. Agapov *et al.*, "Beam dynamics performance of the proposed PETRA IV storage ring," *arXiv*, Aug. 2024. doi:10.48550/arXiv.2408.07995

[19] P. Raimondi *et al.*, "Commissioning of the hybrid multibend achromat lattice at the European Synchrotron Radiation Facility," *Phys. Rev. Accel. Beams*, vol. 24, p. 110701, 2021. doi:10.1103/PhysRevAccelBeams.24.110701

[20] S. M. Liuzzo, "EBS Jan. 2026 restart," presentated at FCC-ee Optics Tuning Meeting, Jan. 2026. https://indico.cern.ch/event/1631087/contributions/6879750/attachments/3203261/5703058/EBS-restart-summary-Jan2026-fcc.pdf

[21] "Conceptual design report for the SOLEIL upgrade," L'Orme des Merisiers, Saint-Aubin, France. https://www.synchrotron-soleil.fr/en/news/conceptual-design-report-soleil-upgrade

[22] S. Habet *et al.*, "Start-to-end commissioning simulations for SOLEIL II storage ring," in *Proc. IPAC'25*, Taipei, Taiwan, Jun. 2025, pp. 698–701. doi:10.18429/JACoW-IPAC2025-MOPS040

[23] K. Oide *et al.*, "Design of beam optics for the Future Circular Collider e^+e^- collider," *Phys. Rev. Accel. Beams*, vol. 19, p. 111005, 2016. doi:10.1103/PhysRevAccelBeams.19.111005

[24] P. Raimondi, M. Hofer, S. Liuzzo, L. Farvacque, and S. White, "Local chromatic correction optics for Future Circular Collider e^+e^-," *Phys. Rev. Accel. Beams*, vol. 28, p. 021002, 2025. doi:10.1103/PhysRevAccelBeams.28.021002

[25] J. Keintzel, R. Tomás *et al.*, "FCC-ee optics tuning – towards the reference design," presented at IPAC'26, Deauville, France, May 2026, paper MOP1039, this conference.